The Meteoritical Society

Meteoritics & Planetary Science 42, Nr 11, 1905–1914 (2007)
Abstract available online at http://meteoritics.org

Laboratory impacts into dry and wet sandstone with and without an overlying water layer: Implications for scaling laws and projectile survivability

E. C. BALDWIN,[1*] D. J. MILNER,[2] M. J. BURCHELL[2], and I. A. CRAWFORD[1]

[1]UCL/Birkbeck Research School of Earth Sciences, University College London, Gower Street, London WC1E 6BT, UK
[2]Centre of Astrophysics and Planetary Science, University of Kent, Canterbury, Kent CT2 7NH, UK
*Corresponding author. E-mail: e.baldwin@ucl.ac.uk

(Received 05 October 2006; Revision accepted 11 July 2007)

Abstract–Scaling laws describing crater dimensions are defined in terms of projectile velocity and mass, densities of the materials involved, strength of the target, and the local gravity. Here, the additional importance of target porosity and saturation, and an overlying water layer, are considered through 15 laboratory impacts of 1 mm diameter stainless steel projectiles at 5 km s^{-1} into a) an initially uncharacterized sandstone (porosity ~17%) and b) Coconino Sandstone (porosity ~23%). The higher-porosity dry sandstone allows a crater to form with a larger diameter but smaller depth than in the lower-porosity dry sandstone. Furthermore, for both porosities, a greater volume of material is excavated from a wet target than a dry target (by 27–30%). Comparison of our results with Pi-scaling (dimensionless ratios of key parameters characterizing cratering data over a range of scales) suggests that porosity is important for scaling laws given that the new data lie significantly beneath the current fit for ice and rock targets on a π_v versus π_3 plot (π_v gives cratering efficiency and π_3 the influence of target strength). An overlying water layer results in a reduction of crater dimensions, with larger craters produced in the saturated targets compared to unsaturated targets. A water depth of approximately 12 times the projectile diameter is required before craters are no longer observed in the targets. Previous experimental studies have shown that this ratio varies between 10 and 20 (Gault and Sonett 1982). In our experiments ~25% of the original projectile mass survives the impact.

INTRODUCTION

Scaling laws to determine crater dimensions are defined in terms of projectile velocity and mass, densities of the materials involved, strength of the target, and the local gravity (e.g., Holsapple and Schmidt 1982, 1987; Melosh 1989; Holsapple 1993). Local conditions, such as the influence of porosity, saturation of the target, and an overlying water layer can also contribute to the nature of crater formation, as discussed below.

Influence of Porosity

Porous targets are known to be poor transmitters of impact shock because their component solids and void spaces present extreme acoustic impedance mismatches. Multiple shock reverberations thus occur at grain boundaries and dissipate the energy into highly localized volume fractions of the target compared to non-porous targets. In addition, the projectile's kinetic energy is partitioned more effectively into target heating, spallation, disruption, and crushing of the grains to fill the void spaces (Love et al. 1993). It would be expected, therefore, that porous targets should displace less material in an impact event. However, natural materials with high porosity often exhibit poor cohesion and generally low compressive yield strengths. The latter effect leads to an increased displaced crater volume per unit incident kinetic energy (as predicted by Holsapple and Schmidt 1987). Love et al. (1993) conducted hypervelocity impacts of soda lime glass projectiles into porous sintered aggregate glass targets and found that increased target porosity leads to deeper crater penetration. This is in contrast to our results (shown later) where the higher porosity target yields a crater that has a larger diameter but smaller depth than a lower porosity target. We also observe that a greater volume of material is excavated from the higher porosity material, whereas Love et al. (1993) observed that the porous targets suffered roughly the same excavated crater volumes than the more competent ones. The difference in dimensions is likely to lie in the differences in strength and densities of the two different targets used, as it is difficult to separate the specific effect of either porosity or strength.

© The Meteoritical Society, 2007. Printed in USA.

Influence of Saturation

Experimental studies have shown that the brittle strength of a rock is reduced in the presence of water (e.g., Baud et al. 2000) and that fluids are likely to change the mode and extent of impact induced failure in rocks (Ahrens and Rubin 1993). Indeed, we have observed experimentally that the presence of water will reduce the yield strength of our sandstone by almost a half (see next section). Although we observe different crater morphologies to Schaefer et al. (2006), we do find that a greater volume (up to 30%) of material is excavated from a wet target than a dry target. It is important to note that Schaefer et al. (2006) performed impact experiments using centimeter-sized projectiles; we have carried out similar impact experiments using millimeter-sized projectiles. Therefore, any differences in the observed output may be attributed to this difference in scale, particularly when considering the scale of the projectile relative to the scale of the grain and/or pore size of the target. Scaling issues have been addressed in more detail later in this paper. For large planetary impacts it may be possible that the target is mechanically disrupted by expanding steam after the passage of the shock wave, which increases the volume and enhances cavity growth in comparison to dry rocks. This interpretation was suggested in a preliminary study by Schaefer et al. (2006).

Influence of an Overlying Water Layer

Given the prevalence of oceans on the Earth, the effect of an overlying water layer on crater dimensions and projectile survivability was also considered in this work. The mechanics of the impact cratering process into water varies somewhat to the standard continental impact model (as described in Melosh 1989). The traverse of the projectile through the water layer will initially cause a void to form within the water; if this cavity is deep enough the projectile will directly impact the ocean floor. The cavity created in the water will collapse giving rise to a central peak of water that will also collapse and propagate out from the impact site, in some cases resulting in a tsunami (e.g., Ward and Asphaug 2000; Gisler et al. 2003; Korycansky 2007). Although the transient crater will form in much the same way as an impact on land, the modification of this crater is significantly different due to the resurge of water into the transient crater cavity. In addition, the water layer significantly slows the projectile prior to impact with the solid target, reducing the peak shock pressures produced both within the projectile and the target site (Artemieva and Shuvalov 2002; Wünnemann and Lange 2002), which are dependent on the vertical component of the projectile's velocity (Pierazzo and Melosh 2000a, 2000b). Consequently, when the water depth is significantly greater than the projectile diameter no crater forms on the ocean floor (e.g., Shuvalov and Trubestkaya 2002). Both laboratory experiments (Gault and Sonett 1982) and detailed numerical simulations (e.g., Shuvalov and Trubestkaya 2002) have shown that there is a critical water depth at which no underwater crater forms, dependent on the target basement material and the parameter d/H, where d is the impactor diameter and H is water depth. Although there is a large difference in velocity between those investigated in the lab (~1–6 km s^{-1}) and those investigated through simulations (~20 km s^{-1}), the critical d/H ratio remains similar for the two techniques. It has been suggested by Shuvalov and Trubestkaya (2002) that the critical d/H ratio is <0.1, a value attributed to work by Gault and Sonett (1982) on loosely consolidated water-saturated sand targets. Interestingly, although the value of 0.1 results from the authors' application of their experiments to a standard impact situation, the experimental data itself indicates that this value is 0.05, i.e., a water-depth-to-projectile-diameter ratio of 20. Gault and Sonett (1982) have also shown experimentally that for velocities of less than 3 km s^{-1} projectile survivability increases with increasing water depth.

In this work, we investigate impacts into saturated and unsaturated sedimentary targets with an overlying water layer for water depths of 0–12 mm, where 12 mm is found to be the limiting water depth for crater formation for our 1 mm projectile diameter impacts. We also present results for projectile survivability at hypervelocities attainable in the laboratory, i.e., ~5 km s^{-1}, which represents the lower regime of hypervelocity planetary impacts.

METHODOLOGY

Initial rock preparation and characterization was carried out in the Rock Physics Laboratory at University College London on two types of sandstone. Our initial experiments used an uncharacterized sandstone for which we determined a 2.18 g cm^{-3} density, typical grain size of 0.4 mm, and a porosity of ~17%. Experiments using this sandstone will be referred to as 'pilot test' sandstone in this work. Subsequent tests used Coconino Sandstone (density = 1.78 g cm^{-3}, typical grain size of 0.15 mm and porosity ~23%) selected for its prevalence at the Meteor Crater impact site (Shoemaker and Kieffer 1974). It has been suggested that the presence of pore water, perhaps related to the proximity of a water table to the impact site, may have influenced the mode in which the target material failed upon impact (Kieffer et al. 1976).

Cylindrical core samples of our pilot test sandstone were cored from the same block and precision-ground to a length of 75 mm and a diameter of 25 mm. The samples were either oven dried to 80 °C lab standard or were saturated in distilled water under a vacuum (pressure = 0.133 Pa) for at least 48 h prior to experimentation. The core samples were used to determine porosities and yield strengths, while blocks 100 × 100 × 60 mm were prepared for the impact experiments. The porosity was determined through the following relationship:

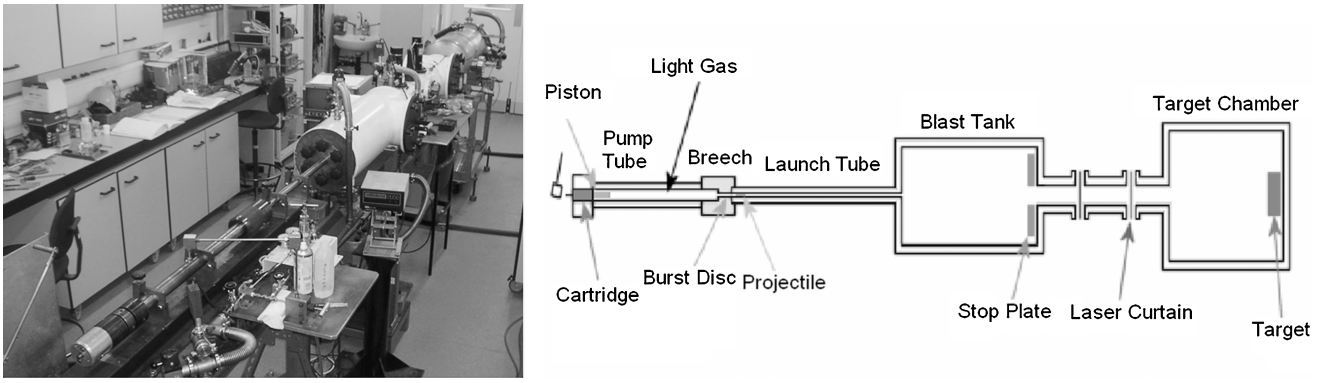


Fig. 1. The University of Kent's two-stage light gas gun (left) and a schematic of the light gas gun (right). The gun is approximately 5 meters in length. For details of its operation, please see Burchell et al. (1999).

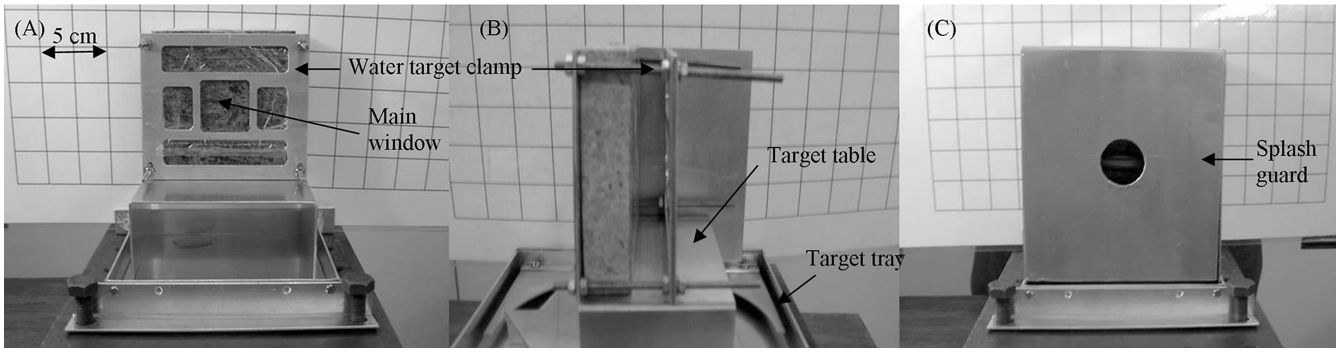


Fig. 2. Series of images showing the water target configuration. a) Face view of the water target. b) Side view of water table and clamp. c) Face view of water target with splash guard. The target holder comprises a water tray used to contain the water after the impact, a target table where the rock target is placed, a water target clamp which holds the water layer in position, and the splash guard which is placed over the target to minimize the amount of water and projectile that can escape during the impact. The target clamp has five windows, the largest of which is the primary target window through which the projectile passes.

$$\Phi = \frac{(m_f - m_i)}{V \rho_{H_2 0}} * 100\% \quad (1)$$

where Φ = porosity, m_f is the saturated (final) mass, and m_i is the unsaturated (initial) mass of the core sample, V is the volume of the core sample, and $\rho H_2 0$ is the density of water. This was repeated twice for each sandstone and an average porosity determined (see Results section). Yield strength experiments were conducted using an unconfined uniaxial compression apparatus (servo-controlled, 200 kN universal load frame) and were performed at a constant strain rate (10^{-5} s^{-1}) until the sample failed. All experiments were carried out under ambient laboratory conditions, with temperatures ~20 °C. The unconfined compressive strength of the cored pilot test sandstone was determined to be 90 MPa for the dry core and 43 MPa for the saturated core. Typical values for the compressive strength of the Coconino Sandstone are approximately 74 MPa for a dry target (Lama and Vutukuri 1978).

The impact shots and analyses were performed at the University of Kent, where the two-stage light gas gun (Burchell et al. 1999) was used to accelerate 1 mm diameter stainless steel 420 projectiles at velocities of approximately 5 km s^{-1}. In all experiments, the target chamber was evacuated to 5 kPa. This is higher than the normal 20–50 Pa that is usually required to prevent deceleration of the projectile in flight. However, it is necessary in the presence of water to use the higher pressure to prevent the water from boiling. Fortunately here, the use of 1 mm projectiles allows a higher target chamber pressure to be used without significant deceleration of the projectile.

The method of target preparation is dependent on whether a water layer is required. When the target does not require a water layer, it is placed into a standard target holder that is secured to the door that opens into the target chamber. When considering an oceanic impact, the target preparation is significantly different (Fig. 2). Given that the light gas gun is not capable of firing vertically, the water is contained in a low density polythene bag (approximately 29 μm in thickness) to prevent it from flowing away prior to the shot. Extensive feasibility testing (Milner 2007) has shown that the bag does not affect the cratering process in any discernible way. The depth of the water layer that the projectile impacts into is varied by adjusting the position of the clamp. The bag containing the water is held firmly in place to prevent it from

Table 1. Crater dimensions produced in sandstone with a two-stage light gas gun. The data for the pilot test sandstone is repeatable; see the data for water depths of 0 mm in Table 3 for comparison.

Sample		Density (g cm^{-3})	Porosity (%)	Crater diameter[a] (mm)	Crater depth[a] (mm)	Crater volume[b] (cm^3)	Impact velocity[c] (km s^{-1})
Pilot test sandstone	Dry	2.18	16.76 ± 0.08	20.50	4.41	0.40	5.03
	Wet	2.35	16.76 ± 0.08	22.28	4.86	0.52	5.08
Coconino Sandstone	Dry	1.78	22.70 ± 0.25	23.87	3.65	1.19	5.10
	Wet	2.01	22.70 ± 0.25	40.01	4.52	1.51	4.90

[a]Accuracy ±0.01 mm; [b]Accuracy ±0.01 cm^3; [c]Accuracy ±1%.

Table 2. Percentage increase in crater dimensions for saturated versus unsaturated targets.

Sandstone	Diameter	Depth	Volume
Pilot test, this work	9%	10%	30%
Coconino, this work	68%	24%	27%
Seeberger, Schaefer et al. (2006)	18%	–20%	54%

bulging out of the target window. The smaller windows are used to the tape the bag in place, ensuring the water depth is uniform across the main window. The windows are also necessary to allow the water to escape in the impact; without them a wave-like surge would propagate through the water layer and potentially deform the target clamp. The target arrangement is placed into the target chamber itself as opposed to being fixed to the chamber door.

ANALYTICAL TECHNIQUES

For all experiments, the crater diameter, depth and volume were analyzed. The crater diameter was determined by using digital callipers to measure the diameter at a number of cross sections. Given the small-scale nature of the impact craters produced in the lab, it is very difficult to separate the effects of spallation from the true impact crater. Through our own estimates we have found that the measured diameter (presented in Table 1) is between 14% and 25% greater than the estimated transient crater diameters for the dry and wet targets, respectively. For the purpose of this paper, and to facilitate comparison to other literature (e.g., Schaefer et al. 2006), we discuss the measured (spallation) diameter.

A 2-D profilometer system was used to measure the depth below the pre-impact surface at 1 mm increments over a cross section of the crater. To determine the volume of the crater cavity we used uniform, fine-grained spherical glass beads with diameters of a few micrometers. The beads were poured into the crater until the cavity was uniformly filled. The mass of beads required to fill the cavity was converted to volume by using a predefined calibration graph (Milner 2007).

For impact events with an overlying water layer, it was possible to retrieve fragments of the projectile after the impact event. The material excavated from the crater was filtered using distilled water and Whatman grade 1 filter paper. The filter paper was then dried using an industrial strength hot air blower. The steel (magnetic) projectile fragments were separated from any rock fragments using a strong magnet, placed in a separate container, and weighed using a fine torsion microbalance (sensitivity ±0.5 ng).

RESULTS AND DISCUSSION

In the first shot program (Tables 1 and 2) two initial experiments used the pilot test sandstone blocks with a density of 2.18 g cm^{-3} (unsaturated) –2.35 g cm^{-3} (saturated) and a porosity of ~17%. Two subsequent tests performed impacts into Coconino Sandstone (density = 1.78 g cm^{-3} [unsaturated] –2.01 g cm^{-3} [saturated] and porosity ~23%), selected for its relevance to the Meteor Crater impact site. In the second shot program (Table 3) eleven further shots were performed into saturated or unsaturated pilot test sandstone with over lying water layers of varying depth. In all cases 1 mm diameter spherical stainless steel 420 projectiles were fired at an average 5.04 km s^{-1} (±0.08 km s^{-1}). Individual velocities for each shot were measured to ±1% (see Burchell et al. 1999) and are recorded in Tables 1 and 3, accordingly. Profiles for all impact craters are shown in Figs. 3–4 (note: vertical scales have been exaggerated).

Influence of a Porous Target

Initial results indicate that the higher porosity sandstone allows a crater with a larger diameter to form than in the lower porosity sandstone, for both saturated and unsaturated scenarios (Table 1). The higher porosity sandstone produces craters of a greater volume than the lower porosity sandstone by a factor of approximately 3. This observed increase in cratering efficiency with target porosity is in conflict with previous experiments (e.g., Love et al. 1993) that produced craters of similar excavated volume despite a wide range in porosity (between 5% and 60%) and subsequently strength. In addition, Love et al. (1993) observed that increased target porosity leads to deeper crater penetration; in our experiments, we find that increased porosity leads to shallower crater depths. Because our results are comparing two porous materials which also have different densities and strengths, this may also influence the observed crater

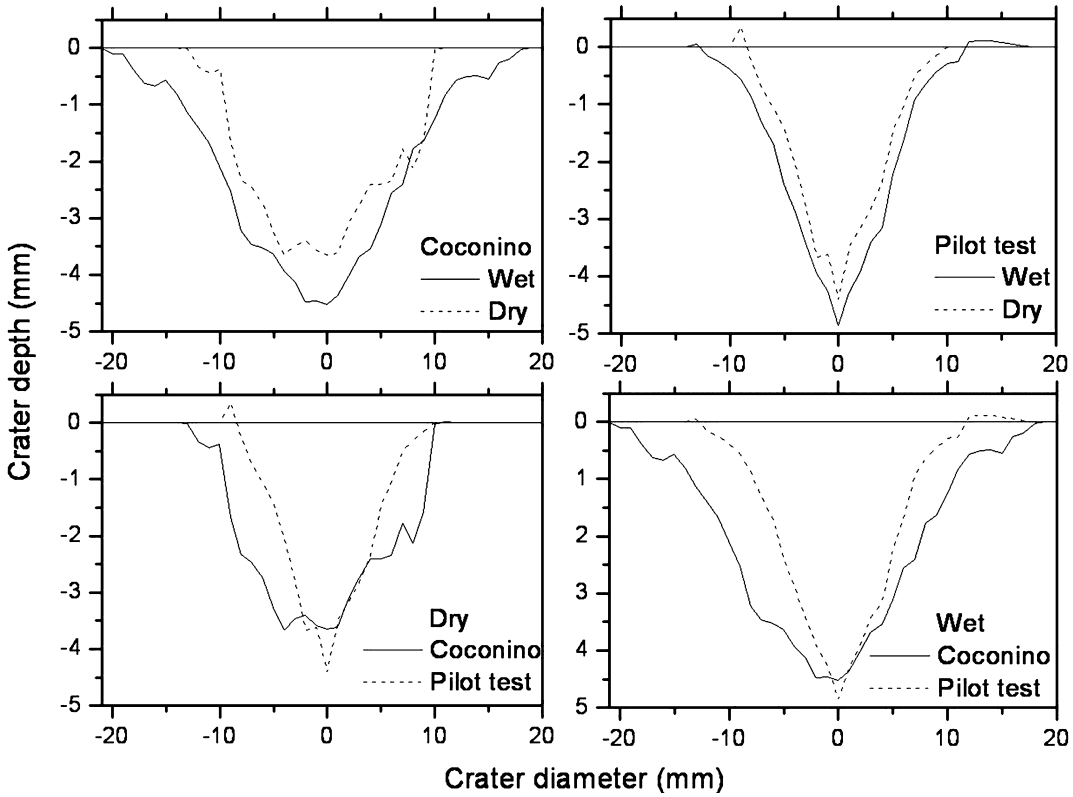


Fig. 3. Plots showing crater profiles in various combinations to compare sandstones of different porosities and saturations using data from Table 1.

dimensions. It is therefore difficult to conclude whether the difference in crater size is solely due to the porosity difference between the two sandstone targets.

Influence of a Saturated Target

We find that under impact, a wet target allows a greater volume of material to be excavated than a dry target (Table 2). Indeed, for both porosities, the crater is wider and deeper in the saturated targets than the unsaturated targets. For the unsaturated experiments, the higher porosity sandstone produces craters 16% wider but 17% shallower than the lower porosity sandstone (Table 1). For the saturated experiments, the higher porosity sandstone produces a crater 79% wider and 6% shallower than the lower porosity sandstone (Table 1). This is perhaps an intuitive outcome given the significantly lower yield strength of wet sandstone to dry sandstone (the pilot test sandstone was found to have a dry strength of 90 MPa but a wet strength of 43 MPa). The dry Coconino Sandstone is quoted as having a dry strength of ~74 MPa (Lama and Vutukuri 1978); it would therefore be reasonable for the wet strength to be roughly half the dry strength. We see that Schaefer et al. (2006) observe a shallower depth and larger diameter in the saturated target than the unsaturated target; for both our sandstone samples, we observe a greater depth in the wet target than the dry. In addition to the different strengths of the sandstones used in these studies, the respective scale of the two experiments may play an important role in this outcome; our experiments were performed with millimeter-scale projectiles while Schaefer et al. (2006) used centimeter-sized projectiles. While the impact velocities in the two experiments were similar (~5 km s^{-1}), the target sandstones have different porosities,

Table 3. Crater dimensions for pilot test sandstone with increasing water depth.

Water depth (mm)[a]	Impact velocity (km s^{-1})[b]	Crater diameter (mm)[c]	Crater depth (mm)[c]	Crater volume (cm^3)[d]
Unsaturated sandstone				
0	5.03	17.03	4.09	0.52
2.5	5.00	12.23	2.85	0.14
5	4.97	10.62	2.42	0.16
7.5	4.98	7.26	1.58	0.073
10	5.22	2.05	0.23	Negligible
Saturated sandstone				
0	4.99	22.30	4.26	0.400
2.5	5.17	13.87	3.68	0.153
5	5.02	12.84	2.25	0.087
7.5	5.11	10.32	1.98	0.033
10	4.96	2.88	0.76	Negligible
12	4.97	1.82	0.24	Negligible

[a]Accuracy ±0.1 mm.
[b]Accuracy ±1%.
[c]Accuracy ±0.01 mm.
[d]Accuracy ±0.007 cm^3.

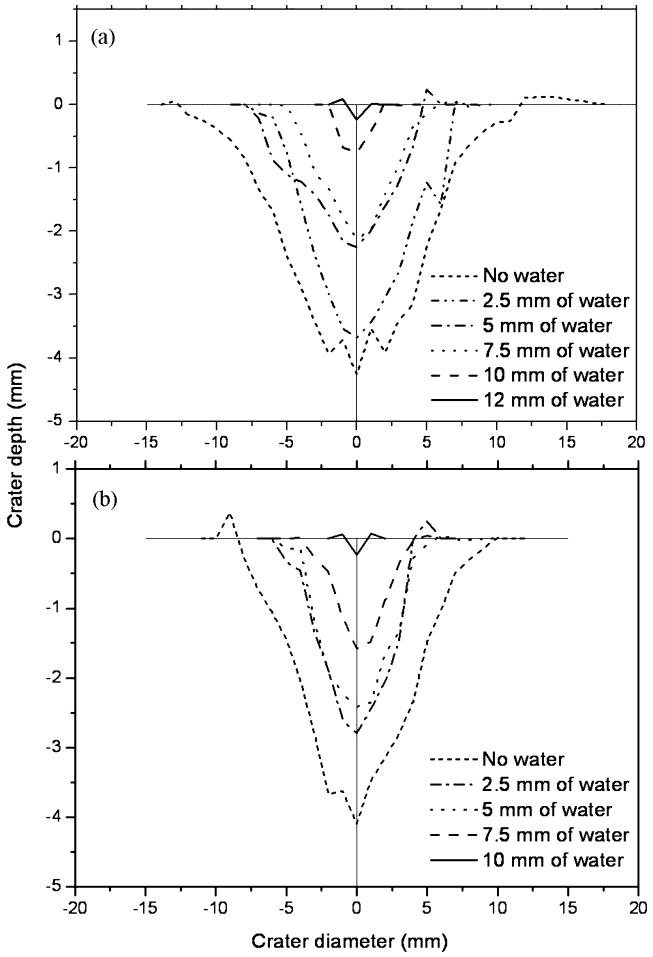


Fig. 4. Crater profiles for (a) saturated sandstone with an overlying water layer of varying depth, and (b) unsaturated sandstone with an overlying water layer of varying depth using data from Table 3. For the saturated sandstone, no crater is observed when the water depth is >12 mm, for the unsaturated sandstone no crater is observed when the water depth is >10 mm. At these limiting values only a scar on the rock surface is observed.

and, in addition, Schaefer et al.'s (2006) target is layered in porosity, ranging from 12–20%, and is only 44% saturated whereas ours are close to 100% saturated. Variable porosity and saturation, and the effect this may have on crater formation, may provide the focus for future modeling attempts.

Influence of an Overlying Water Layer

Oceanic impacts are represented in the laboratory by impacting 1 mm diameter stainless steel projectiles into sandstone targets with overlying layers of water up to 12 mm deep. In general, a saturated target enhances crater growth; crater dimensions decrease linearly as water depth increases, for both saturated and unsaturated targets (Figs. 5 and 6), while crater volumes follow an exponential decrease with increasing water depth (Fig. 7). By extrapolating the fits in

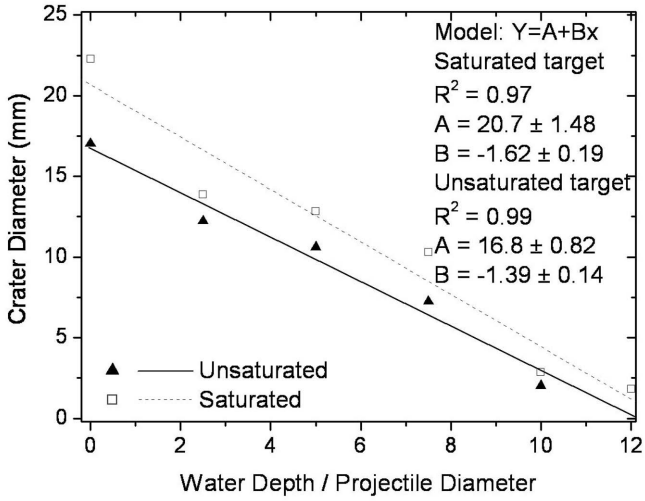


Fig. 5. Decrease in crater diameter for increasing water depth for (□) saturated and (▲) unsaturated sandstone targets. For raw data see Table 3. R^2 is the square of the regression coefficient and indicates a good fit was obtained. The value A is the maximum crater diameter (mm) achieved with no overlying water layer. The value B is the gradient of the linear fit. When focusing on crater diameter, no observable crater can be detected when the water-depth-to-projectile-diameter ratio is 12.8 ± 0.6 for the saturated sandstone and 12.1 ± 0.64 for the unsaturated sandstone.

Figs. 5 and 6 to the point at which no crater forms, it can be seen that an average water depth of 11.6 ± 0.5 times the projectile diameter prevents crater formation in the unsaturated target; the corresponding value for a saturated target is 12.7 ± 0.6. This lies within the water-depth-to-projectile-diameter ratio range predicted by Gault and Sonett (1982) and Shuvalov and Trebestkaya (2002). However, Gault and Sonett (1982) derived their prediction based on experiments into sand, a much weaker material than the sandstone used in our experiments. Indeed, the experimental data of Gault and Sonett points to a *d*/H value of 0.05, therefore our values are consistent with the idea that strength plays an important role in this value, i.e., a stronger target requires a larger *d*/H ratio to prevent cratering than loosely consolidated strata. Other factors can influence this ratio, such as impact angle and projectile density and composition. For example, it would be reasonable to expect a nickel-iron asteroid (density = 7000–8000 kg m^{-3}) to create a larger impact crater than a typical chondritic impactor (density = 3400 kg m^{-3}), therefore more dense impactors may require a greater water depth for this *d*/H limit to be achieved. Our projectile material is stainless steel, comparable in density to an iron impactor, therefore our results are likely to represent an upper limit to the *d*/H ratio, when considering only projectile material.

The change in scale of the impact from lab to planetary scale may also affect the *d*/H value, given that the strength of the rock typically decreases as the loading duration increases. Because loading times increase with the size

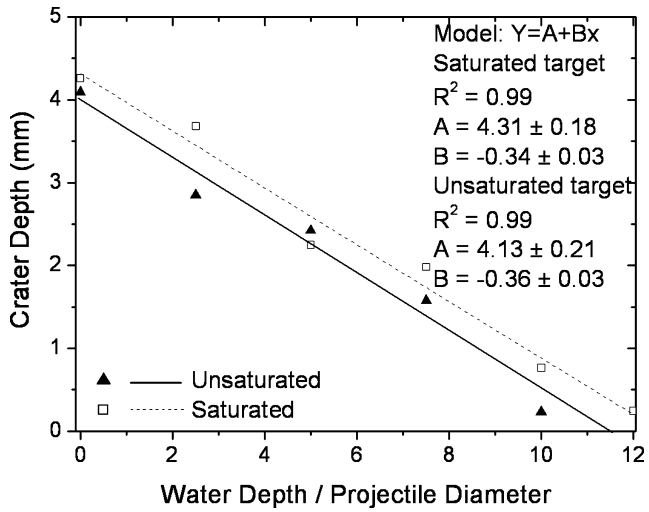


Fig. 6. Decrease in crater depth for increasing water depth for (□) saturated and (▲) unsaturated sandstone targets. For raw data see Table 3. R^2 is the square of the regression coefficient and indicates a good fit was obtained. The value A is the maximum crater depth (mm) achieved with no overlying water layer. The value B is the gradient of the linear fit. When focusing on crater depth, no observable crater can be detected when the water-depth-to-projectile-diameter ratio is 12.7 ± 0.6 for the saturated sandstone and 11.2 ± 0.36 for the unsaturated sandstone.

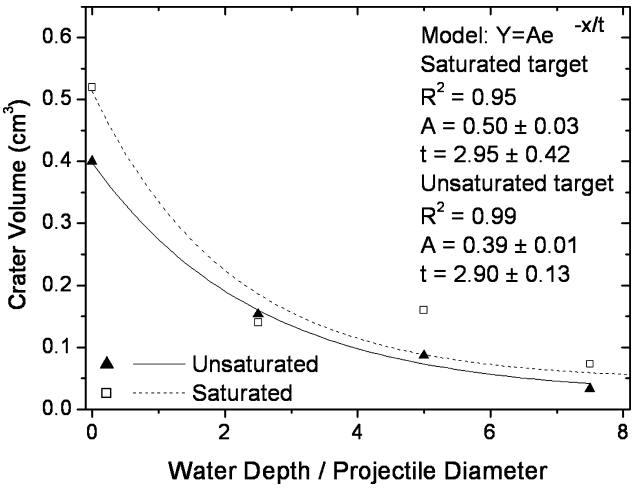


Fig. 7. Decrease in crater volume for increasing water depth for (□) saturated and (▲) unsaturated sandstone targets. For raw data see Table 3. R^2 is the square of the regression coefficient and indicates a good fit was obtained. The value A is the maximum crater volume (cm^3) achieved with no overlying water layer. The value t controls the rate of decay of the exponential fit.

scale of the impact event, larger targets are effectively weaker than smaller ones (e.g., Housen and Holsapple 1999). Indeed, Housen and Holsapple (1999) have shown that for collision tests where the kinetic energy per unit target mass and impact velocity were kept constant, the target damage became increasingly severe as the size scale increased—a result of effective weakening of the target at larger size scales. We can therefore postulate that our lab specimens are actually stronger than their large-scale counterparts. This would suggest that for impacts into water the critical *d*/H value could in fact be smaller for large impacts than for lab ones. In addition, for loosely consolidated materials such as sand, there is undoubtedly a gravity-related component of crater formation. However, the late-time growth of an underwater crater is also dominated by gravity, so in both strength and gravity-dominated bottom materials it is likely that there is a scale dependence in the critical *d*/H ratio.

Projectile Survivability

For impacts with a water layer present, we detect partial projectile survivability in all scenarios investigated in this work. If a crater is produced, however, fragments of the surviving projectile become fused to the sandstone grains, producing large uncertainties in analyzing the surviving mass. For the saturated target with a 12 mm deep "ocean," only scarring of the sandstone occurred, therefore there was no contamination of the projectile fragments. In this case, we extracted ~25% of the original mass of the projectile. It may be expected, therefore, that a significant amount of material may also survive a planetary-scale impact into water. Moreover, while material interpreted as fragments of the parent meteorite have been recovered from large oceanic impacts such as Eltanin (Kyte 2002), a recent discovery has shown that fragments can also survive impact into a continental basement, as found in the Morokweng crater, South Africa (Maier et al. 2006). For our dry impacts, projectile survivability could not be estimated due to the surviving projectile fragments being fused into sandstone grains, preventing uncontaminated projectile extraction. Projectile survivability at a planetary scale is discussed in more detail later in the paper.

Pi-SCALING

A common approach to impact crater scaling is through Pi-group scaling, a technique that is based upon determining the relationships between dimensionless ratios of the parameters which are involved in the impact process (Melosh 1989). These include the transient crater diameter D_t, crater volume V, target and projectile densities ρ_t and ρ_p, planetary gravity g, projectile mass m, impact velocity v_i and target strength Y. The main relationships are defined as:

$$\pi_D = D_t \left(\frac{\rho_t}{m}\right)^{1/3} \tag{2}$$

$$\pi_2 = \frac{1.61 g L}{v_i^2} \tag{3}$$

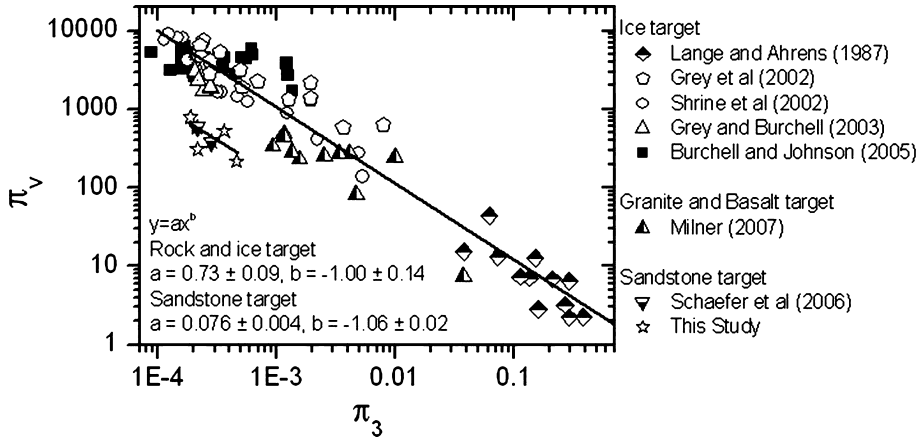


Fig. 8. Pi-scaled data for π_3 versus π_v, see text for further explanation.

$$\pi_3 = \frac{Y}{\rho_p v_i^2} \tag{4}$$

$$\pi_4 = \frac{\rho_t}{\rho_p} \tag{5}$$

where π_D is a dimensionless measure of the crater diameter, π_2 represents the gravity-controlled cratering regime, π_3 is the strength-controlled cratering regime, and π_4 is the ratio of target and projectile densities. For experimental research, data is generally presented in terms of the volume excavated or mass displaced from a crater. The dimensionless parameter π_v is then defined as:

$$\pi_v = \frac{\rho_t V}{m} \tag{6}$$

This quantity is the ratio between the mass displaced from the crater ($\rho_t V$) and the mass of the projectile (m), and is commonly referred to as the cratering efficiency. Given that we have performed experiments at the lab scale, our craters are dominated by the strength regime, hence we use the π_3 relation to compare with the cratering efficiency π_v. This is comparable to extensive research conducted for impacts onto ice (e.g., Burchell and Johnson [2005] and references therein) and competent rock (e.g., Milner 2007). Our results are presented alongside these results in Fig. 8. From Fig. 8 it can be seen that the fit to the rock and ice data is of the form $\pi_v = a\ \pi_3{}^b$, where the constants a and b are 0.73 and −1, respectively. However, the data for the sandstone lies significantly beneath this trend, while maintaining a similar gradient. This suggests that the factor b remains similar while the factor a is reduced by an order of magnitude. It is difficult to determine b accurately due to the limit in the range of π_3, and consequently more data points over a larger range are required to determine the reliability of this result.

Interestingly, it was highlighted by Melosh (1989) that the Pi-group scaling neglects some information regarding material properties. This was originally thought to be the angle of internal friction of the target material, but experiments and theoretical studies now support the idea that porosity is the missing term. The angle of internal friction may still play a role, particularly for granular materials such as sand, regolith or soils, as illustrated in Melosh (1989) for the gravity regime where sand forms a distinctly separate trend line to those which represent water, limestone, competent rock, and saturated soil targets (which all lie close to each other). In addition, it was also highlighted by Burchell and Johnson (2005) that no detailed consideration of how a porous target may change the Pi-scaling relationships themselves, other than by lowering the target density, had really been considered in great detail. Therefore, our results strengthen the argument for considering porosity as a critical factor in deriving universal scaling laws. The missing porosity term (defined as π_5 after Melosh [1989]) would be required in the Pi-group equations to ensure similarity between all materials, i.e., between porous and non-porous materials. Based on our very initial observations of where the new sandstone targets lie on this graph, it is apparent that π_v requires multiplication; for the trend line shown here, this equates to a factor of 10. For non-porous materials this multiplication factor would be 1. This is obviously only a very preliminary observation based on just a few sandstone samples. In future work, we will investigate a wider range of velocities and other porous materials to cover a larger range of π_3 values. It would also be insightful to study sandstones with either similar porosity but different strength, or similar strengths but different porosities, in an attempt to separate the effect these two parameters have on the proposed π_5 term.

Implications for Large Planetary Impacts

While it is with some caution that laboratory impact events can be directly scaled to large planetary impacts, we can draw on our results to make predictions for the influence of porosity, saturation and an overlying water layer on crater

formation and projectile survivability in planetary impacts. Indeed, while many numerical models produce excellent agreement with observed crater morphology, the restrictive nature of material modeling generally precludes consideration of initial material conditions such as water saturation. It is only recently that porosity has been noted as an important consideration for modeling impacts into asteroids (Housen and Holsapple 2003); it is also an extremely important consideration when attempting to model and understand impacts into sedimentary basements, for example the Meteor Crater impact site. To this end, attempts are being made to implement a better representation of porosity effects into numerical codes (e.g., Wünnemann et al. 2006). Also relevant to Meteor Crater is the presumed presence of a water table, which may in part have caused the impact site to be partially saturated (Kieffer et al. 1976), perhaps reducing the strength of the target and affecting the way in which it failed under impact.

The consideration of an overlying water layer in the laboratory is of indubitable importance to terrestrial cratering, given the greater area of ocean to land creating a bias towards oceanic impacts. Where most of the projectile is destroyed in a continental impact, significant proportions of the projectile remain in an oceanic impact. This has important implications for both the successful delivery of extraterrestrial organic material to the Earth (Milner et al. 2006) and for the theory of panspermia (Melosh 1988; Burchell 2004). However, it is possible that as the projectile scales from laboratory to planetary impact sizes, there may be changes in both the fraction of projectile that survives intact and the size distribution of the fragments. Moreover, and as previously discussed, the effect that size scaling has on the strength of the target will affect the interpolation of the *d*/H ratio to planetary scale. Based on the assumptions of Housen and Holsapple (1999), we can infer that our lab specimens are actually stronger than their large-scale counterparts. This would imply that, for impacts into water, the critical *d*/H value could in fact be smaller for large impacts than for lab ones. In addition, insight into how much energy remains at the point of impact on the ocean floor after the projectile has been decelerated by the water column would further our understanding on how this effects the *d*/H ratio. The interaction between the impactor and the water column at a planetary scale is explored through numerical modelling by Wünnemann and Lange (2002). Unfortunately, details of the extent of deceleration on the projectile by the water column have yet to be determined in the lab, although the process is probably similar to the way in which a projectile is slowed by an atmosphere, as discussed by Melosh (1989) and Chyba et al. (1993). Many of the issues in scaling could be addressed with detailed hydrocode modeling, but appropriate input would have to be made for the influence of porosity.

CONCLUSIONS

We show through experimental techniques that target porosity and saturation affect resultant crater dimensions. Our experiments reveal that higher porosity targets and saturated targets yield a larger crater than lower porosity targets. When interpreting our sandstone results with Pi-scaling, we find that both our results and that of Schaefer et al. (2006) lie below the trend line of non-porous materials, when considering the strength regime of crater scaling. Although it is difficult to isolate the individual effect of porosity on crater formation due to the differing strengths and densities of the targets used in this study, it is likely that porosity is a strong influencing factor of where the sandstone data points lie, as postulated in Melosh (1989), and because the π_3 term already accounts for differences in target strength and density. In future work we will investigate a wider range of velocities and other porous materials to cover a larger range of π_3 values. It would also be insightful to study sandstones with either similar porosity but different strength, or similar strengths but different porosities, in an attempt to separate the effect these two parameters have on the proposed π_5 term.

When considering impact events where a water layer is present, we observe an approximately linear decrease in crater dimensions and an exponential decrease in crater volume, with larger craters forming where a saturated target provides the basement. Previous results show that a maximum water depth-to-projectile-diameter of 20 is required (Gault and Sonett 1982, based on a sand target) to prevent an underwater crater from forming; we show that this value is much lower, approximately 12, for sandstone targets, and indeed varies slightly depending on whether the target is saturated or unsaturated. This suggests that the water-depth-to-projectile-diameter ratio limitation on cratering is variable dependant upon the target material. For example, the *d/H* ratio may vary for the deeper ocean (where there is a dense, basaltic ocean floor) compared to the shallower continental edge (where sediments overlying a crystalline basement exist). These different situations will provide the basis for future investigation in the lab.

For our impact into a deep water layer, where cratering is prohibited, we find that ~25% of the original projectile mass survives the impact. Despite the orders of magnitude difference between laboratory and planetary impacts, these findings tentatively suggest that an abundant amount of extraterrestrial material could have survived impact onto the Earth's ocean surface, perhaps providing a suitable mechanism for successful panspermia.

Acknowledgments–We thank Neil Hughes for preparing the blocks of sandstone, Michael Heap for preparing core samples and for directing rock characterization techniques, and Mike Cole for firing the light gas gun. We also thank our

reviewers Kai Wünnemann and Kevin Housen, and the associate editor Alex Deutsch, for their constructive comments and careful reviews, which significantly improved an earlier version of this manuscript.

Editorial Handling—Dr. Alexander Deutsch

REFERENCES

Ahrens T. J. and Rubin A. M. 1993. Impact-induced tensional failure in rock. *Journal of Geophysical Research* 98:1185–1203.

Artemieva N. A. and Shuvalov V. V. 2002. Shock metamorphism on the ocean floor (numerical simulations). *Deep Sea Research II* 49:959–968.

Baud P., Zhu W., and Wong T. 2000. Failure mode and weakening effect of water on sandstone. *Journal of Geophysical Research* 105:16371–16389.

Burchell M. J. 2004. Panspermia today. *International Journal of Astrobiology* 3:73–80.

Burchell M. J., Cole M. J., McDonnell J. A. M., and Zarnecki J. C. 1999. Hypervelocity impact studies using the 2MV Van der Graff accelerator and two-stage light gas gun of the University of Kent at Canterbury. *Measurements Science and Technology* 10:41–50.

Burchell M. J. and Johnson E. 2005. Impact craters on small icy bodies such as icy satellites and comet nuclei. *Monthly Notices of the Royal Astronomical Society* 360:769–781.

Chyba C. F., Thomas P. J., and Zahnle K. J. 1993. The 1908 Tunguska explosion: Atmospheric disruption of a stony asteroid. *Nature* 361:40–44.

Gault D. E. and Sonett C. P. 1982. Laboratory simulation of pelagic asteroid impact: Atmospheric injection, benthic topography, and the surface wave radiation field. In *Geological implications of impacts of large asteroids and comets on the Earth,* edited by Silver L. T. and Schultz P. H. GSA Special Paper #190. Boulder, Colorado: Geological Society of America. pp. 69–92.

Gisler G., Weaver R., and Mader C. 2003. Two and three dimensional simulations of asteroid ocean impacts. *Science of Tsunami Hazards* 21:119–134.

Grey I. D. S., Burchell M. J., and Shrine N. R. G. 2002. Scaling of hypervelocity impact craters in ice with impact angle. *Journal of Geophysical Research* 107, doi:10.1029/2001JE001525.

Grey I. D. S. and Burchell M. J. 2003. Hypervelocity impact cratering on water ice targets at temperatures ranging from 100 K to 253 K. *Journal of Geophysical Research* 108, doi: 10.1029/2002/JE001899.

Holsapple K. A. 1993. The scaling of impact process in planetary sciences. *Annual Reviews of Earth and Planetary Science* 21: 333–373.

Holsapple K. A. and Schmidt R. M. 1982. On the scaling of crater dimensions 2. Impact processes. *Journal of Geophysical Research* 87:1849–1870.

Holsapple K. A. and Schmidt R. M. 1987. Point source solutions and coupling parameters in cratering mechanics. *Journal of Geophysical Research* 92:6350–6376.

Housen K. R. and Holsapple K. A. 1999. Scale effects in strength-dominated collisions of rocky asteroids. *Icarus* 142:21–33.

Housen K. R. and Holsapple K. A. 2003. Impact cratering on porous asteroids. *Icarus* 163:102–119.

Kieffer S., Phakey P. P., and Christie J. M. 1976. Shock processes in porous quartzite: Transmission electron microscope observations and theory. *Contributions to Mineralogy and Petrology* 59:41–93.

Korycansky D. G. 2007. Runup from impact tsunami—Further results (abstract #1227). 38th Lunar and Planetary Science Conference. CD-ROM.

Kyte F. T. 2002. Unmelted meteoritic debris collected from Eltanin ejecta in Polarstern cores from expedition ANT XII/4. *Deep Sea Research II* 49:1063–1071

Lange M. A. and Ahrens T. J. 1987. Impact experiments in low-temperature ice. *Icarus* 69:506–518.

Lama R. D. and Vutukuri V. S. 1978. Appendix II: Laboratory mechanical properties of rocks. In *Handbook on mechanical properties of rocks,* vol. 2, edited by Wöhlbier H. Bay Village, Ohio: Trans Tech Publications. pp. 315–465.

Love S. G., Hörz F., and Brownlee D. E. 1993. Target porosity effects in impact cratering and collisional disruption. *Icarus* 105:216–224.

Maier W. D., Andreoli M. A. G, McDonald I., Higgins M. D., Boyce A. J., Shukolyukov A., Lugmair G. W., Aswell L. D., Graser P., Ripley E. M., and Hart R. J. 2006. Discovery of a 25 cm asteroid clast in the giant Morokweng impact crater, South Africa. *Nature* 441:203–206.

Melosh H. J. 1988. A rocky road to Panspermia. *Nature* 322:687–688.

Melosh H. 1989. *Impact cratering—A geological process*. New York: Oxford University Press. 245 p.

Milner D. J. 2007. Simulations of oceanic impact events. Ph.D. thesis, University of Kent, Canterbury, UK. 236 p.

Milner D. J., Burchell M. J., Creighton J. A., and Parnell J. 2006. Oceanic hypervelocity impact events: A viable mechanism for successful panspermia? *International Journal of Astrobiology* 5:261–268.

Pierazzo E. and Melosh H. J. 2000a. Hydrocode modelling of oblique impacts: The fate of the projectile. *Meteoritics & Planetary Science* 35:117–130.

Pierazzo E. and Melosh H. J. 2000b. Melt production in oblique impacts. *Icarus* 145:252–261.

Schaefer F., Thoma K., Behner T., Nau S., Kenkmann T., Wünnemann K., Deutsch A., and the MEMIN Team. 2006. Impact experiments on dry and wet sandstone. *Proceedings of the ESLAB-40: First International Conference on Impact Cratering in the Solar System.* ESA Special Publication #612.

Shoemaker E. M. and Kieffer S. W. 1974. Guidebook to the geology of Meteor Crater, Arizona. Tempe, Arizona: Arizona State University. pp. 1–11.

Shrine N. R. G., Burchell M. J., and Grey I. D. S. 2002. Velocity scaling of impact craters in water ice over the range 1–7.3 km/s. *Icarus* 155:475–485.

Shuvalov V. V. and Trubestkaya I. A. 2002. Numerical modelling of marine target impacts. *Solar System Research* 36:417–430.

Ward S. N. and Asphaug E. 2000. Asteroid impact tsunami: A probabilistic hazard assessment. *Icarus* 145:64–78.

Wünnemann K., Collins G. S., and Melosh H. J. 2006. A strain-based porosity model for use in hydrocode simulations of impacts and implications for transient crater growth in porous targets. *Icarus* 180:514–527.

Wünnemann K. and Lange M. A. 2002. Numerical modeling of impact-induced modifications of the deep-sea floor. *Deep Sea Research II* 49:969–981.